# Vector lifting scheme for phase-shifting holographic data compression

Yafei Xing, Mounir Kaaniche, Béatrice Pesquet-Popescu, Frédéric Dufaux

# Vector lifting scheme for phase-shifting holographic data compression

**Yafei Xing,[a] Mounir Kaaniche,[b] Béatrice Pesquet-Popescu,[a] Frédéric Dufaux[a]**
[a]Institut Mines-Télécom, Télécom ParisTech, CNRS LTCI, 37-39 Rue Dareau, Paris, France, 75014
[b]Université Paris 13, Sorbonne Paris Cité, L2TI-Institut Galilée, 99 avenue J. B. Clément, Villetaneuse, France, 93430

**Abstract.** With the increasing interest for holography in 3D imaging applications, the use of hologram compression techniques is mandatory for storage and transmission purposes. The state-of-the-art approach aims at encoding separately each interference pattern by resorting to common still image compression techniques. Contrary to such an independent scheme, a novel joint hologram coding scheme is investigated in this paper. More precisely, instead of encoding all the interference patterns, it is proposed to compress only two sets of data, by taking into account the redundancies existing among them. The resulting data are encoded by applying a joint multiscale decomposition based on the vector lifting concept. Experimental results show the benefits which can be drawn from the proposed hologram compression approach.

**Keywords:** Digital holograms, phase-shifting, object reconstruction, compression, wavelets, lifting schemes.

**Address all correspondence to**: Yafei Xing, Institut Mines-Télécom, Télécom ParisTech, CNRS LTCI, 37-39 Rue Dareau, Paris, France, 75014; Tel: +33 1 45 81 73 27; Fax: +33 1 45 81 71 44; E-mail: yafei.xing@telecom-paristech.fr

## 1 Introduction

With the growing expectation of three-dimensional (3D) experience, interest for 3D video is steadily gaining momentum. Current 3D techniques are mainly based on stereoscopic and multiview representations, which only exploit limited depth cues. Furthermore, they inherently introduce an accommodation-vergence conflict, which may induce headache, nausea or visual fatigue. Instead, considered as the ultimate 3D imaging technology, holography[1–3] is able to offer the potential of all depth cues by fully reconstructing the wavefront of the object or scene. Giving the advantages of CCD sensor and computer calculation, digital holography (DH)[4,5] and computer generated holography (CGH),[6,7] have also been developed with promising features.

In CGH, hologram is generated by mathematically simulating the optical wave propagation with different computational techniques. Several issues need to be addressed for synthesizing,

processing, compressing and transmitting CGHs. The first one consists in deciding mathematical models of the object and geometry of wave propagation from objects to the hologram plane. The second one is related to the computation of the interference patterns by carrying out discrete transformations on the object fields. The third one is the design of a suitable representation and compression of the interference patterns, which is referred to as hologram encoding.

Generally speaking, the geometry of wave propagation is related to the selected objects. When objects are represented using "geometrical" models where objects are composed of elementary elements, interference patterns are computed as a superposition of elementary holograms. Ray tracing method is suitable for 3D objects consisting of scatter points .[8] By simply tracing the ray from a point source to a sampling point on the hologram, it is the most flexible method for synthesizing CGHs.

Raster graphic models, such as bitmap images, are the most general objects that can be easily obtained. Due to some natural limitations of visual observation, the observation surface can be considered as composed of small sub-areas approximated by planes having the same distance to the CCD sensor or the eyes. Under such assumptions, some mathematical models have been developed, of which two important and commonly used ones are Fresnel holograms and Fourier holograms.[9] Both of them are based on Discrete Fourier transforms.

In DH and CGH, one of the main problems is to find a suitable representation and effective compression in order to reduce the very high data rate. The representation of digital holograms is either composed of real and imaginary information, or amplitude and phase information. However, using in-line setup[1] or off-axis setup,[10] the reconstructed objects always suffer from zero-order image and twin image. For this reason, in-line phase-shifting digital holography (PSDH) proposed by Yamaguchi[11] is more practical for avoiding both zero-order image and twin image by using

reference wave with stepwise changed phase. According to the specificity of PSDH, the intensities of three interference patterns are applied to reconstruct objects. However, the extra amount of CGHs and the calculation of the complex object wavefront required by the phase-shifting algorithm proves more costly in terms of data storage or transmission. Thus, effective compression methods of holographic data become an issue of importance.

To this end, different techniques have been developed. Some work has focused on the wavefront by coding separately its real and complex components.[12] Moreover, compression of the interference patterns has been suggested in[13] by applying common still image compression techniques like JPEG and JPEG2000. Finally, compression of phase-shifting holographic data has also been proposed by using a family of wavelets.[14–16] In a recent work,[17] it was shown that it is more interesting to encode two sets of difference data that contain the effective holographic information.

In this paper, a novel and efficient compression scheme for phase-shifting holographic data is developed. Indeed, to the best of our knowledge, the reported hologram compression methods consist generally in independently encoding each pattern (or component). Since the generated patterns correspond physically to the same 3D object, the different representations present redundancies, that will be exploited by encoding *jointly* the phase-shifting holographic data based on a vector lifting decomposition. More specifically, an optimized structure, which is adapted to the content of the holograms, is designed.

This paper is organized as follows. In Section 2, the main issues regarding digital holography and an overview of hologram compression methods are addressed. The proposed joint hologram coding scheme based on the vector lifting concept is described in Section 3. Finally, experimental results are given in Section 4 and some conclusions are drawn in Section 5.

## 2 State-of-the art on Digital Holography

### *2.1 Computer Generated Phase-Shifting Holography*

The CGHs are generated by simulating the physical digital holograms recording procedure of in-line PSDH. The basic setup is illustrated in Fig. 1(a). A laser beam is split into two paths by a beam splitter (BS), one of which illuminates an object and interferes with the other beam, which is also called reference beam, at the CCD sensor. The reference beam is reflected at the piezoelectric transducer (PZT) mirror that phase modulates the beam by a computer. By shifting the phase of the reference beam with a constant, different holograms are obtained to derive the complex amplitude of the object wave.

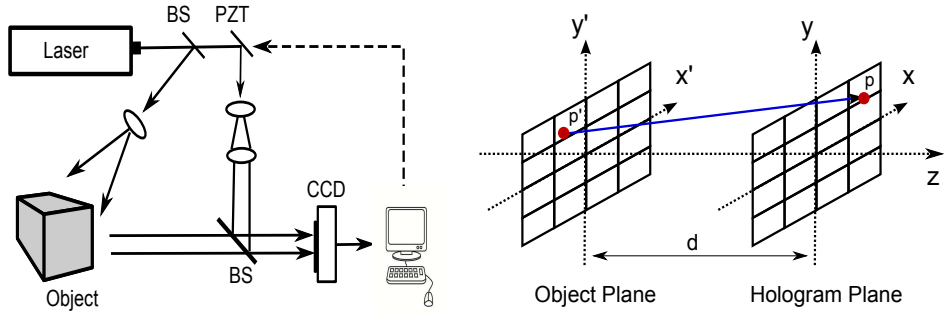


(a) (b)

**Fig 1** (a) Setup for phase-shifting digital holography: BS: beam splitters; PZT, piezoelectric transducer mirror; (b) Co-ordinate system of hologram recording.

Mathematical models for generating holograms are related to the chosen object models. Hereafter, Fresnel transform method with bitmap image objects is selected. The coordinate system can be simplified as in Fig. 1(b). The object plane is parallel to the hologram plane. Assuming the object points are located at ($x'$,$y'$) in the object plane, then the object wave at the hologram plane is represented by

$$U(x,y) = \int\int U_o(x',y') \exp[\imath kd + \imath k\frac{(x-x')^2+(y-y')^2}{2d}]dx'dy' \tag{1}$$

where integration is carried out over infinity, $U_o(x', y')$ denotes the complex amplitude of the object point, $k = \frac{2\pi}{\lambda}$ is the wave number, $\lambda$ is the wavelength of the laser beam and $d$ is the distance between the object plane and the hologram plane $(d > 0)$.

Using Fresnel transform, Eq. (1) can be approximated as follows:[18]

$$U(x, y) = \exp[\imath\frac{\pi}{\lambda d}(x^2 + y^2)]\mathscr{F}\{U_o(x', y') \exp[\imath\frac{\pi}{\lambda d}(x')^2 + (y')^2]\} \tag{2}$$

where $\mathscr{F}$ denotes the Fourier transform. Afterwards, the object wave is superimposed upon the phase-shifted reference wave whose complex amplitude is expressed by:

$$U_R(x, y, \phi) = A_R(x, y) \exp(\imath\phi) \tag{3}$$

where $\phi$ is the phase and $A_R$ is the amplitude of the phase shifted reference wave. By assuming that the initial phase $\phi$ of reference wave is zero and changes by $\frac{\pi}{2}$ each step, the resulting intensity of the interference pattern is computed as follows:

$$I_H(x, y; \phi) = |U_R(x, y; \phi) + U(x, y)|^2, \qquad \phi \in \{0, \frac{\pi}{2}, \pi\} \tag{4}$$

### *2.2 Numerical Object Reconstruction*

Objects reconstructed by PSDH no longer suffer from zero-order image and twin image. The reason is that the complex amplitude of the object wavefront at the hologram plane can be calculated directly using CGHs in the case of a three-step algorithm[19] by Eq. (5):

$$\widehat{U}(x, y) = \frac{1 - \imath}{4U_R^*}\{I_H(x, y; 0) - I_H(x, y; \frac{\pi}{2}) + \imath[I_H(x, y; \frac{\pi}{2}) - I_H(x, y; \pi)]\} \tag{5}$$

where $U_R^*$ is the conjugate of the reference wave with $\phi = 0$.

Image reconstruction is performed by the inverse Fresnel transformation of the derived complex amplitude $\widehat{U}(x, y)$.

### *2.3 Existing hologram compression methods*

In order to reduce the storage and transmission burden of holographic data, especially phase-shifting holographic data, numerous lossless and lossy compression methods have been developed. In Ref. 12, lossless techniques such as Lempel-Ziv, Lempel-Ziv-Welch, Huffman and Burrows-Wheeler,[20] are used to encode separately real and complex components of data streams, and lossy compression techniques such as subsampling and quantization of Fourier coefficients are applied to interference patterns. Due to the low spatial redundancies of hologram's speckle nature, lossless compression methods are usually inefficient.[13] As a result, most of the earlier work has been devoted to the lossy compression context.

Quantization was firstly introduced in PSDH by Mills and Yamaguchi.[21] However, this approach reduces the effectiveness of compression as well as the resulting quality. Indeed, as the number of bits decreases, the quality falls rapidly. The use of Fresnelets for PSDH compression has been studied in Ref. 15. It consists first in decomposing the complex wavefront to Fresnelet coefficients, and then applying an uniform subband quantization. Experimental results show that it can be used very effectively for the compression of holographic data. Moreover, based on scalar quantization, Arrifano *et al.* developed a multiple description coding (MDC) method on DHs using a maximum-a-posteriori technique.[22] It takes advantage of MDC for optimally coding data between available channels and mitigate channel errors, which turns out to be a powerful mechanism. Furthermore, investigation of vector quantization based on LBG algorithm on computer

generated phase-shifting holographic (CGPSH) data has been conducted recently in our previous work.[17] Instead of compressing CGPSH data directly, two sets of effective holographic information are extracted and encoded, which result in a reduction of the raw data rate due to their inherent redundancies. Furthermore, it has been shown that better performance is obtained using vector quantization compared to adaptive scalar quantization.

Compression of phase-shifting holographic data by standard JPEG and JPEG 2000 compression techniques has been addressed in Ref. 14, with reported compression ratios in the range of 20 to 27, at acceptable reconstruction levels. Similarly, in our previous work,[16] compressing CGPSH data by standard JPEG and JPEG2000 techniques has been investigated.

A 3D scanning method has been introduced in Ref. 23. More specifically, interference patterns have been divided into blocks, and 2D DCT has been performed. The resulting segments have been scanned in 3D, in order to form a sequence which was then compressed using a combination of advanced video coding, differential pulse code modulation and lossless coding. High compression rates have been reported. The use of MPEG-4 Advanced Simple Profile (ASP) for the compression of hologram sequences was investigated by Darakis.[24] Higher performance was obtained by MPEG-4 ASP inter-frame coding in the proposed approach, compared to independent intra-frame coding.

## 3 Proposed joint coding scheme

### *3.1 Motivation*

Since the interference patterns are generated from the wavefronts emanating from the same 3D object, the resulting holograms present similar visual contents. Thus, it is expected that these kinds of data show redundancies, and from this point of view, efficient hologram compression

schemes can be designed by exploiting the dependencies between these patterns. To this end, it is proposed here to apply the Vector Lifting concept which was found to be an efficient compression tool in the context of stereo and multispectral data.[25,26]

### *3.2 Vector Lifting Scheme (VLS)*

Firstly, note that the generated interference patterns are real-valued grayscale images. In this section, the two input dependent images to be encoded are denoted by $S^{(1)}$ and $S^{(2)}$. Before describing VLS, let us recall that most of the existing joint coding schemes, which have been developed in the literature for video and stereo/multiview data compression purpose, consist of two steps. First, one image (for example $S^{(1)}$) is selected as a reference image and encoded independently of the other one. Then, the second image $S^{(2)}$, selected as a target image, is predicted from the first one $S^{(1)}$, and the difference between the two images, called the residual, is encoded. Typically, Discrete Cosine Transform (DCT) or Discrete Wavelet Transform (DWT) can be used for encoding both the reference and residual images.[27,28]

Contrary to this standard scheme, the main feature of VLS is that it does not generate a residual image, but two compact representations of the images $S^{(1)}$ and $S^{(2)}$. For the sake of simplicity, a separable vector lifting structure, whose block diagram is illustrated in Fig. 2, is considered in this paper.

Therefore, the principle of this multiscale decomposition will be described for a given line $x$. In what follows, $S_j^{(1)}$ and $S_j^{(2)}$ designate the approximation coefficients of $S^{(1)}$ and $S^{(2)}$ at each resolution level $j$. While $j = 0$ corresponds to the initial (full resolution) images $S^{(1)}$ and $S^{(2)}$, note that the dimensions of $S_j^{(1)}$ and $S_j^{(2)}$ ($j \geq 1$) are divided by $2^j$ along the horizontal and vertical directions.

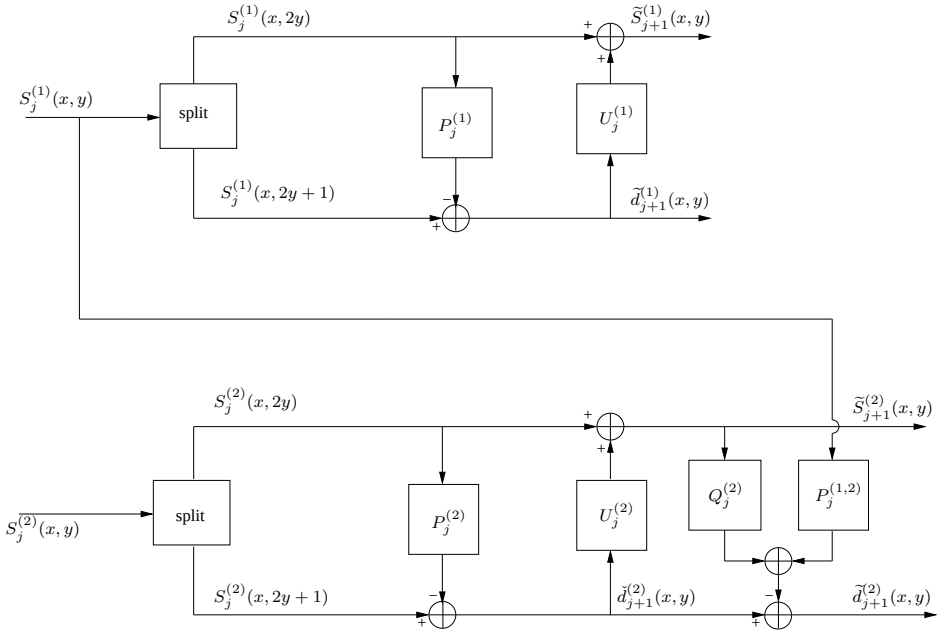


**Fig 2** Principle of the VLS decomposition.

As it can be seen in Fig. 2, the reference image $S^{(1)}$ is firstly encoded using a classical lifting structure[29–32] composed of a prediction and an update stage. To this end, for a given line $x$, the input signal $S_j^{(1)}(x,y)$ is firstly partitioned into two data sets formed by the even $S_j^{(1)}(x,2y)$ and odd samples $S_j^{(1)}(x,2y+1)$, respectively. Then, during the prediction step, each sample of one of the two subsets (say the odd ones) is predicted from the neighboring even samples, yielding the detail coefficients $\widetilde{d}_{j+1}^{(1)}$ at the resolution $(j+1)$:

$$\widetilde{d}_{j+1}^{(1)}(x,y) = S_j^{(1)}(x,2y+1) - \sum_{k \in \mathcal{P}_j^{(1)}} p_{j,k}^{(1)} S_j^{(1)}(x,2y-2k) \tag{6}$$

where the coefficients $p_{j,k}^{(1)}$ and the set $\mathcal{P}_j^{(1)}$ represent respectively the weights and the support of the predictor of the odd samples $S_j^{(1)}(x,2y+1)$. After that, the update step aims at computing a coarser approximation $\widetilde{S}_{j+1}^{(1)}$ of the original image by smoothing the even sample $S_j^{(1)}(x,2y)$ as

follows:

$$\widetilde{S}_{j+1}^{(1)}(x,y) = S_j^{(1)}(x,2y) + \sum_{k \in \mathcal{U}_1^{(1)}} u_{j,k}^{(1)} \widetilde{d}_{j+1}^{(1)}(x,y-k), \tag{7}$$

where the set $\mathcal{U}_j^{(1)}$ denotes the spatial support of the update operator whose coefficients are $u_{j,k}^{(1)}$. Once the reference image $S^{(1)}$ is encoded in intra mode like the standard scheme, the attention will be paid now to the target image $S^{(2)}$. It is important to note that the main difference between a basic lifting scheme and the vector lifting scheme is that for the target image $S^{(2)}$, the prediction step uses samples from the same image and *also* their corresponding pixels taken from the reference image $S^{(1)}$. As shown in Fig. 2, a P-U-P structure is used for the target image $S^{(2)}$. More precisely, a first intra-prediction step is applied to generate an intermediate detail signal $\check{d}_{j+1}^{(2)}$, which will serve to compute the approximation signal $\widetilde{S}_{j+1}^{(2)}$ through the update step. After that, an hybrid prediction is performed by exploiting *simultaneously* the intra and inter-image redundancies in order to compute the final detail signal $\widetilde{d}_{j+1}^{(2)}$. Thus, the resulting decomposition implies the following equations:

$$\check{d}_{j+1}^{(2)}(x,y) = S_j^{(2)}(x,2y+1) - \sum_{k \in \mathcal{P}_j^{(2)}} p_{j,k}^{(2)} S_j^{(2)}(x,2y-2k), \tag{8}$$

$$\widetilde{S}_{j+1}^{(2)}(x,y) = S_j^{(2)}(x,2y) + \sum_{k \in \mathcal{U}_j^{(2)}} u_{j,k}^{(2)} \check{d}_{j+1}^{(2)}(x,y-k), \tag{9}$$

$$\widetilde{d}_{j+1}^{(2)}(x,y) = \check{d}_{j+1}^{(2)}(x,y) - \Big( \sum_{k \in \mathcal{Q}_j} q_{j,k} \widetilde{S}_{j+1}^{(2)}(x,y-k) + \sum_{k \in \mathcal{P}_j^{(1,2)}} p_{j,k}^{(1,2)} S_j^{(1)}(x,2y+1-k) \Big) \tag{10}$$

where $\mathcal{P}_j^{(2)}$ (resp. $\mathcal{P}_j^{(1,2)}$) is the spatial support of the intra-image (resp. inter-images) whereas its weights are designated by $p_{j,k}^{(2)}$ (resp. $p_{j,k}^{(1,2)}$), and $\mathcal{Q}_j$ (resp. $q_{j,k}$) is the support (resp. weights) of

the second intra-image predictor.

Since a separable decomposition has been considered, these steps are iterated on the columns $y$ of the resulting subbands $\widetilde{S}_{j+1}^{(1)}$, $\widetilde{d}_{j+1}^{(1)}$, $\widetilde{S}_{j+1}^{(2)}$ and $\widetilde{d}_{j+1}^{(2)}$ in order to produce the approximation subbands $S_{j+1}^{(1)}$ and $S_{j+1}^{(2)}$ as well as three details subbands, for each image, oriented horizontally, vertically and diagonally. This decomposition is again repeated on the approximation subbands over $J$ resolution levels, yielding the multiresolution representation of the two input images.

Finally, at the last resolution level $J$, instead of encoding the approximation subband of the target image $S_J^{(2)}$, it is proposed to encode the residual subband given by:

$$e_J^{(2)}(x,y) = S_J^{(2)}(x,y) - \sum_{k \in \mathcal{P}_J^{(1,2)}} p_{J,k}^{(1,2)} S_J^{(1)}(x, y-k). \tag{11}$$

### *3.3 Proposed hologram compression method based on VLS*

According to the description of phase-shifting algorithm, Eq. (5) states that only the intensity of the three patterns $I_H(x,y;\phi)$, with $\phi \in \{o, \frac{\pi}{2}, \pi\}$, is needed for the object wave reconstruction. This intensity information can be rewritten as:

$$I_H(x,y;\phi) = A_R^2(x,y) + A^2(x,y) + 2A_R(x,y)A(x,y)\cos(\phi(x,y) - \varphi(x,y)), \tag{12}$$

where $A(x,y)$ and $\varphi(x,y)$ are the amplitude and phase of object wave at point $(x,y)$, respectively. Moreover, according to Eq. (5), the effective holographic information is composed of the difference between $I_H(x,y;0)$ and $I_H(x,y;\frac{\pi}{2})$ on the one hand, and between $I_H(x,y;\frac{\pi}{2})$ and $I_H(x,y;\pi)$ on the other hand. Therefore, instead of encoding three sets of intensity data, it is sufficient to encode only two sets. In what follows, two encoding procedures are proposed.

*3.3.1 Procedure-1*

The first method aims at encoding the difference data $D^{(1)}$ and $D^{(2)}$ given by:

$$\begin{cases} D^{(1)}(x,y) = I_H(x,y;0) - I_H(x,y;\frac{\pi}{2}) \\ \\ D^{(2)}(x,y) = I_H(x,y;\frac{\pi}{2}) - I_H(x,y;\pi) \end{cases} \tag{13}$$

Before illustrating these kinds of data, Fig. 3 displays the 6 virtual 3D objects used in this work.

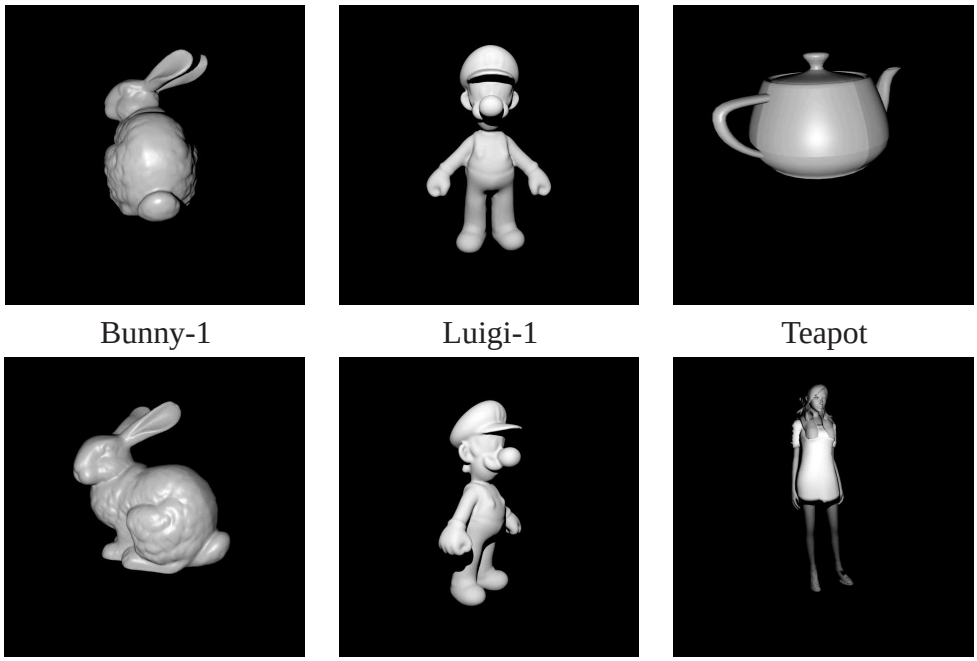


**Fig 3** Different test 3D objects

As an example, Fig. 4 shows the data $(D^{(1)}, D^{(2)})$ for the "Luigi-1" object. It can be noticed that the obtained difference data present visually similar patterns. To confirm this, Table 1 provides for some objects the entropy measure[33] computed on the original image $D^{(2)}$, the residual one $D^{(2)} - D^{(1)}$, and the error resulting from a joint prediction similar to VLS, which is denoted in Table 1 by $D^{(2)} - Pred(D^{(1)}, D^{(2)})$. Thus, by generating the prediction error, the entropy has been

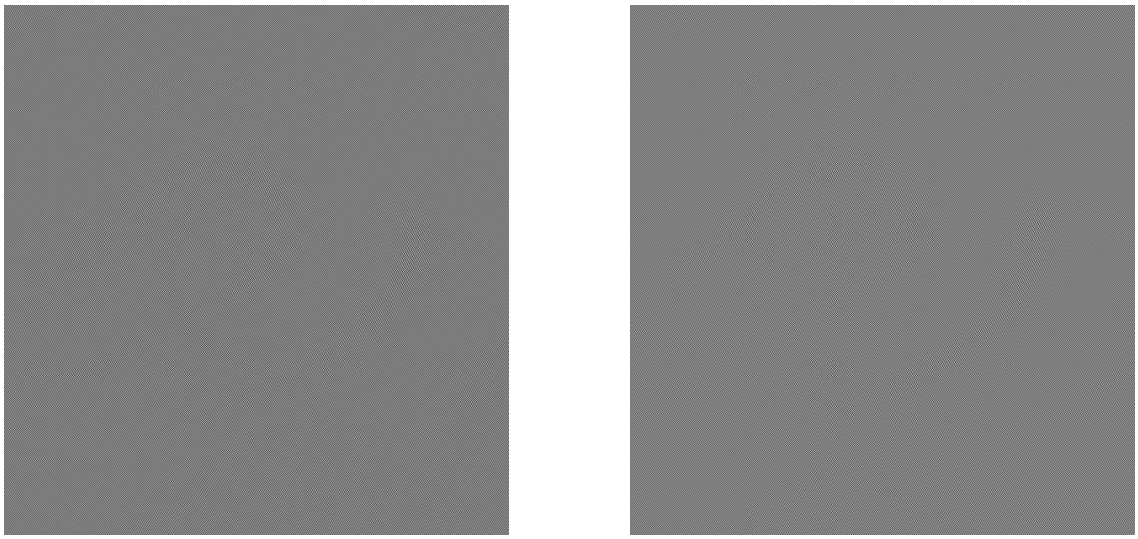

$D^{(1)}$ $D^{(2)}$

**Fig 4** Example of two difference data $D^{(1)}$ and $D^{(2)}$ for the "Luigi-1" object.

decreased which confirms the redundancies existing between $D^{(1)}$ and $D^{(2)}$. For this reason, it has been proposed in this paper to encode $D^{(1)}$ and $D^{(2)}$ using the VLS.

More precisely, $D^{(1)}$ will be encoded in intra-mode by using Eqs. (6) and (7) to compute the wavelet coefficients. To this end, a prediction and update filters with spatial supports $\mathcal{P}_j^{(1)} = \{-1, 0\}$ and $\mathcal{U}_j^{(1)} = \{0, 1\}$ are considered. In addition, the weights of the update filter are set for all the resolution levels to: $u_{j,0}^{(1)} = u_{j,1}^{(1)} = \frac{1}{4}$. However, it is proposed to optimize the prediction weights $p_{j,-1}^{(1)}$ and $p_{j,0}^{(1)}$ in order to design a coding scheme well adapted to the contents of the hologram data. More specifically, these prediction filter coefficients are optimized at each resolution level $j$ by minimizing the variance of the detail signal $\widetilde{d}_{j+1}^{(1)}$.

**Table 1** Entropy measure on $D^{(2)}$, $D^{(2)} - D^{(1)}$ and $D^{(2)} - Pred(D^{(1)}, D^{(2)})$ of "Luigi-1", "Luigi-2" and "Girl" objects

| Objects | $D^{(2)}$ | $D^{(2)} - D^{(1)}$ | $D^{(2)} - Pred(D^{(1)}, D^{(2)})$ |
|---|---|---|---|
| Luigi-1 | 27.32 | 27.31 | 23.65 |
| Luigi-2 | 25.99 | 25.85 | 18.77 |
| Girl | 25.98 | 26.11 | 13.29 |

Concerning the second signal $D^{(2)}$, the same intra-prediction and update filters used with $D^{(1)}$ will be employed to generate the signals $\check{d}_{j+1}^{(2)}$ and $\widetilde{D}_{j+1}^{(2)}$. Then, the second prediction stage is performed by setting $\mathcal{Q}_j = \{-1, 0\}$ and $\mathcal{P}_j^{(1,2)} = \{-1, 0, 1\}$ for $j \in \{0, \ldots, J-1\}$ and $\mathcal{P}_J^{(1,2)} = \{0\}$. The coefficients $q_{j,k}$ and $p_{j,k}^{(1,2)}$ are also optimized by minimizing the variance of the detail signal $\widetilde{d}_{j+1}^{(2)}$.

### *3.3.2 Procedure-2*

Now, instead of encoding the difference data $D^{(1)}$ and $D^{(2)}$, another strategy can be applied. Indeed, by further exploring the intensity information $I_H(x, y; \phi)$, it can be noticed that the third term of Eq. (12), $2A_R(x, y)A(x, y)\cos(\phi(x, y) - \varphi(x, y))$, contains all effective information in the sense that the first and second terms of Eq. (12) will be eliminated during the subtraction operations in Eq. (13). Thus, by only retaining the third term, three signals can be defined as follows:

$$\begin{aligned} I^{(1)}(x, y) &= 2A_R(x, y)A(x, y)\cos(0 - \varphi(x, y)) \\ &= 2A_R(x, y)A(x, y)\cos(\varphi(x, y)) \end{aligned} \tag{14}$$

$$\begin{aligned} I^{(2)}(x, y) &= 2A_R(x, y)A(x, y)\cos(\frac{\pi}{2} - \varphi(x, y)) \\ &= 2A_R(x, y)A(x, y)\sin(\varphi(x, y)) \end{aligned} \tag{15}$$

$$\begin{aligned} I^{(3)}(x, y) &= 2A_R(x, y)A(x, y)\cos(\pi - \varphi(x, y)) \\ &= -I^{(1)}(x, y) \end{aligned} \tag{16}$$

Note that $D^{(1)}$ and $D^{(2)}$ given by Eq. (13) can be re-expressed as follows:

$$\begin{cases} D^{(1)}(x, y) = I^{(1)}(x, y) - I^{(2)}(x, y) \\ D^{(2)}(x, y) = I^{(1)}(x, y) + I^{(2)}(x, y) \end{cases} \tag{17}$$

By looking to $I^{(1)}$ and $I^{(2)}$, it can observed that they present also visually similar patterns as shown in Fig. 5. Therefore, instead of encoding $D^{(1)}$ and $D^{(2)}$, one can also directly encode $I^{(1)}$

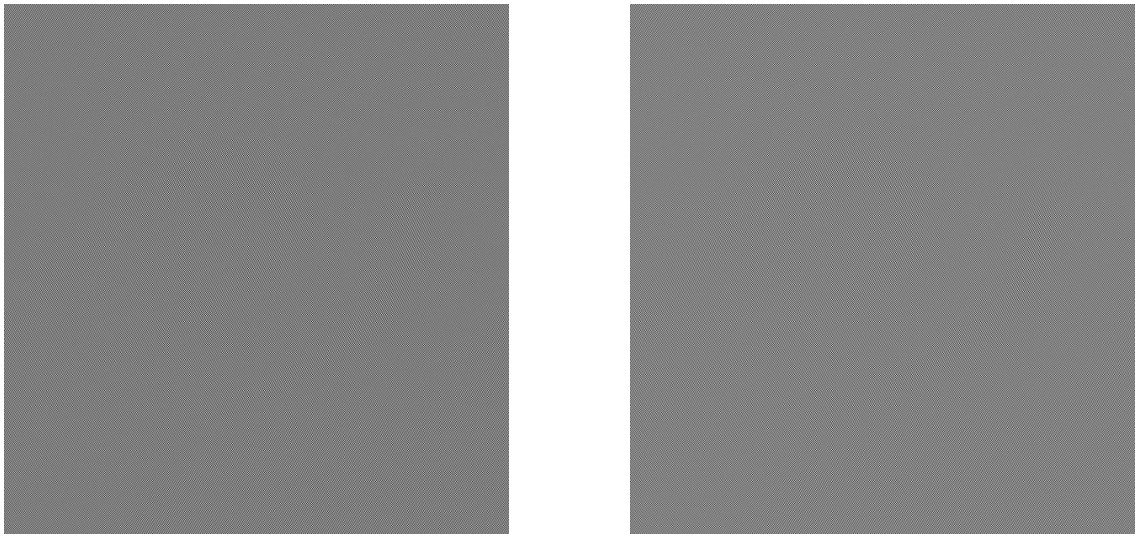

$I^{(1)}$ $I^{(2)}$

**Fig 5** Example of $I^{(1)}$ and $I^{(2)}$ for the Bunny-1 object.

and $I^{(2)}$ by using the VLS. While the same spatial supports of the prediction and update filters used previously to encode $D^{(1)}$ and $D^{(2)}$ are considered, it is important to note that the prediction weights are re-optimized and adapted to the contents of $I^{(1)}$ and $I^{(2)}$.

Obviously, at the decoder side, the decoded images $\widehat{I}^{(1)}$ and $\widehat{I}^{(2)}$ are firstly determined for a given bitrate, and then, the associated difference signals used for the object wave reconstruction can be deduced:

$$\begin{cases} \widehat{D}^{(1)}(x,y) = \widehat{I}^{(1)}(x,y) - \widehat{I}^{(2)}(x,y) \\ \widehat{D}^{(2)}(x,y) = \widehat{I}^{(1)}(x,y) + \widehat{I}^{(2)}(x,y) \end{cases} \tag{18}$$

It should be noted that the resulting distortions of $D^{(1)}$ and $D^{(2)}$ can be obtained from that of $I^{(1)}$ and $I^{(2)}$ as follows:

$$\begin{aligned}
&\mathsf{E}\{(I^{(1)} - \widehat{I}^{(1)})^2\} + \mathsf{E}\{(I^{(2)} - \widehat{I}^{(2)})^2\} \\
&= \mathsf{E}\{(I^{(1)} - \frac{1}{2}(\widehat{D}^{(1)} + \widehat{D}^{(2)}))^2\} + \mathsf{E}\{(I^{(2)} - \frac{1}{2}(\widehat{D}^{(2)} - \widehat{D}^{(1)}))^2\} \\
&= \frac{1}{4}\Big(\mathsf{E}\{(D^{(1)} + D^{(2)} - \widehat{D}^{(1)} - \widehat{D}^{(2)})^2\} + \mathsf{E}\{(D^{(2)} - D^{(1)} - \widehat{D}^{(2)} + \widehat{D}^{(1)})^2\}\Big) \\
&= \frac{1}{2}\Big(\mathsf{E}\{(D^{(1)} - \widehat{D}^{(1)})^2\} + \mathsf{E}\{(D^{(2)} - \widehat{D}^{(2)})^2\}\Big) \qquad (19)
\end{aligned}$$

## 4 Experimental results

### *4.1 Computer Generated Holography Setup*

Based on the fact that the whole procedure of CGH is numerical, and with the assumption that the number of samples ($N_x \times N_y$) in the object plane is equal to that of the hologram plane for simplicity, Eq. (2) is subsequently digitally represented as:

$$U(k,l) = exp[\imath\frac{\pi}{\lambda d}(k^2(\Delta x')^2 + l^2(\Delta y')^2)] * \mathscr{F}\{\widehat{U}_o(m,n)exp[\imath\frac{\pi}{\lambda d}(m^2\Delta x^2 + n^2\Delta y^2)]\} \qquad (20)$$

where $k = 1, 2, ..., N_x$, $l = 1, 2, ..., N_y$ and $m = 1, 2, ..., N_x$, $n = 1, 2, ..., N_y$ are the discrete dimensions' indices of the hologram and object planes, respectively; $\Delta x$, $\Delta y$ and $\Delta x'$, $\Delta y'$are the sampling intervals in horizontal and vertical directions of the hologram and object planes,

respectively. Due to the bandwidth limitation, they satisfy the following requirements:

$$\begin{aligned} \Delta x &= \frac{\lambda d}{L_x + L_{x'}}, \qquad \Delta y = \frac{\lambda d}{L_y + L_{y'}} \\ \Delta x' &= \frac{\lambda d}{N_x \Delta x}, \qquad \Delta y' = \frac{\lambda d}{N_y \Delta y} \end{aligned} \tag{21}$$

where $L_x \times L_y$ and $L_{x'} \times L_{y'}$ are the dimensions of the hologram and object planes, respectively. Table 2 describes some basic setup for CGPSH.

**Table 2** Parameters of CGPSH

| | |
|---|---|
| laser wavelength | $\lambda = 630nm$ |
| distance of two planes | $d = 0.55m$ |
| dimension of hologram plane | $L_x \times L_y = 5.5mm \times 5.5mm$ |
| number of samples | $N_x \times N_y = 600 \times 600$ |

### *4.2 Simulations and discussion*

Simulations are performed on 6 virtual 3D objects which have been already illustrated in Fig. 3. In order to show the benefit of the proposed hologram compression scheme based on VLS, the following methods are considered:

• The first one corresponds to the state-of-the-art hologram compression method where the inputs $I^{(1)}$ and $I^{(2)}$ (or $D^{(1)}$ and $D^{(2)}$) are separately encoded by using existing still image coders.[14,16] To this end, JPEG2000[34] is used in its lossy compression mode with the 9/7 wavelet transform. It is worth pointing out that this independent scheme has been retained for comparison because, in the previous work,[17] it has been shown that this scheme is more performant than the conventional hologram compression approach where the three interference patterns are separately encoded.

• The second one is the standard joint coding scheme, explained at the beginning of Section 3, where a reference and a residual image are also encoded using JPEG2000 and the 9/7 transform.

Note that this technique has been considered in most of joint coding schemes developed in the context of stereo and video data compression.[28]

• The third one corresponds to the proposed joint coding scheme based on the vector lifting concept, applied either to the pair of correlated differences $(D^{(1)}, D^{(2)})$ or to the pair $(I^{(1)}, I^{(2)})$.

All these decompositions are carried out over three resolution levels. In what follows, these schemes will be respectively designated by Independent-I (resp. Independent-II), Standard-I (resp. Standard-II) and VLS-I (resp. VLS-II) when $D^{(1)}$ and $D^{(2)}$ (resp. $I^{(1)}$ and $I^{(2)}$) are encoded.

The entropy measure introduced in Section 3.3.1, is indeed a good estimate of the coding performance of these different schemes as shown in Table 3. Different from Table 2, Table 3 evaluates the entropy measure based on the wavelet decomposition of the correspondent data in Table 2, which corresponds to the designation of Independent-I, Standard-I and VLS-I, respectively. The decreased entropy obtained by VLS-I confirms the efficiency of VLS-I for predicting redundancies. However, the performance of these methods are mainly compared in terms of the standard PSNR criterion as well as the perceptual metric SSIM[35] of the reconstructed 3D object.

**Table 3** Entropy measure of three different compression schemes on "Luigi-1", "Luigi-2" and "Girl" objects

| Objects | Independent-I | SSD-I | VLS-I |
|---|---|---|---|
| Luigi-1 | 21.14 | 20.82 | 17.98 |
| Luigi-2 | 22.06 | 21.62 | 16.58 |
| Girl | 19.36 | 19.43 | 15.10 |

The first part has focused on the encoding of the difference data $D^{(1)}$ and $D^{(2)}$. Figures 6 and 7 illustrate the rate-distortion results in terms of PSNR and SSIM versus the bitrate given in bit per pixel (bpp). It can be firstly noticed that the standard scheme is less performant than the conventional independent scheme where the inputs are independently encoded. This may explain the fact that residual-based coding methods have not been reported earlier, and it has been preferred to

encode separately each pattern. However, the proposed coding method based on VLS outperforms the two other methods. Compared to the standard coding scheme (resp. the independent one), the PSNR and SSIM improvements range from 2-4 dB (resp. 1-2 dB) and 0.2-0.3 (resp. 0.1-0.2). In addition, Figures (8)-(11) display some reconstructed objects at different bitrates. It can be observed that VLS leads to the best visual quality of the reconstruction.

Next, the second strategy which aims at encoding $I^{(1)}$ and $I^{(2)}$ instead of $D^{(1)}$ and $D^{(2)}$ has also been tested. In this case, the resulting PSNR and SSIM of the reconstructed objects are given in Figures 12 and 13. By comparing these results to those obtained in Figures 6 and 7, it can be deduced that encoding the pairs $(D^{(1)}, D^{(2)})$ and $(I^{(1)}, I^{(2)})$ lead generally to similar performance. Whatever the encoded set of data, all these results confirm the effectiveness of the proposed joint coding scheme based on VLS for holographic data compression purposes.

## 5 Conclusion

This work has been devoted to the compression of phase-shifting holographic data. More precisely, instead of encoding the three interference patterns classically used to represent these data, only a set of two derived data is encoded. To this end, a new joint multiscale decomposition based on the vector lifting concept has been developed. Moreover, the proposed coding scheme has been adapted to the contents of the hologram data. Experimental results have indicated the good performance of the proposed approach over the conventional ones in terms of quality of the reconstructed 3D object. A significant gain of about 2 dB and 0.15 in terms of PSNR and SSIM, respectively, has been achieved compared to the state-of-the-art independent coding scheme.

It is worth pointing out that the developed VLS has been performed in a separable way by cascading the 1D decomposition along the horizontal direction, then along the vertical direction. However,

according to the visual patterns of the difference data $D^{(1)}$ and $D^{(2)}$, it can be noticed that these signals present some structures (similar to the propagation of waves) which are neither horizontal nor vertical. Thus, it would be interesting to develop a non separable decomposition to better exploit the characteristics of the hologram data. Moreover, the proposed scheme can be extended to a digital holographic video coding framework.

*References*


1 D. Gabor, "A new microscopic principle," *Nature* **161**(4098), 777–778 (1948).

2 L. Onural, A. P. Gotchev, H. M. Ozaktas, and E. Stoykova, "A survey of signal processing problems and tools in holographic three-dimensional television," *IEEE Transactions on Circuits and Systems for Video Technology* **17**(11), 1631–1647 (2007).

3 B. Javidi, P. Ferraro, S.-H. Hong, S. D. Nicola, A. Finizio, D. Alfieri, and G. Pierattini, "Three-dimensional image fusion by use of multiwavelength digital holography," *Optics Letters* **30**, 144–146 (2005).

4 U. Schnars and W. Jüptner, "Direct recording of holograms by a CCD target and numerical reconstruction," *Applied Optics* **33**, 179–181 (1994).

5 J. W. Goodman and R. W. Lawrence, "Digital image formation from electronically detected holograms," *Physics Letters* **11**, 77–79 (1967).

6 W. J. Dallas, "Computer-generated holograms," in *The Computer in Optical Research*, B. Frieden, Ed., *Topics in Applied Physics* **41**, 291–366, Springer Berlin Heidelberg (1980).

7 G. Tricoles, "Computer generated holograms: an historical review," *Applied Optics* **26**, 4351–4357 (1987).

8 A. D. Stein, Z. Wang, and J. S. Leigh, "Computer-generated holograms: A simplified ray-tracing approach," in *Computers in Physics*, 389–392 (1992).

9 D. Abookasis and J. Rosen, "Fourier, Fresnel and image CGHs of three-dimensional objects observed from many different projections," in *Proceedings of SPIE, Interferometry XII: Techniques and Analysis,*, **5531**, 273–284 (2004).

10 E. N. Leith and J. Upatnieks, "Reconstructed wavefronts and communication theory," *Journal of the Optical Society of America* **52**, 1123–1128 (1962).

11 I. Yamaguchi and T. Zhang, "Phase-shifting digital holography," *Optics Letters* **22**, 1268–1270 (1997).

12 T. J. Naughton, Y. Frauel, B. Javidi, and E. Tajahuerce, "Compression of digital holograms for three-dimensional object reconstruction and recognition," *Applied Optics* **41**(20), 4124–4132 (2002).

13 E. Darakis, T. J. Naughton, J. J. Soraghan, and B. Javidi, "Measurement of compression defects in phase-shifting digital holographic data," in *Proc. SPIE, Optical Information Systems IV*, **6311** (2006).

14 E. Darakis and J. J. Soraghan, "Compression of interference patterns with application to phase-shifting digital holography," *Applied Optics* **45**, 2437–2443 (2006).

15 E. Darakis and J. Soraghan, "Use of fresnelets for phase-shifting digital hologram compression," *IEEE Transactions on Image Processing* **15**(12), 3804–3811 (2006).

16 Y. Xing, B. Pesquet-Popescu, and F. Dufaux, "Compression of computer generated phase-shifting hologram sequence using AVC and HEVC," in *Proc. SPIE, Applications of Digital Image Processing XXXVI*, **8856**, (San Diego, California, USA) (2013).

17 Y. Xing, B. Pesquet-Popescu, and F. Dufaux, “Vector quantization for computer generated phase-shifting holograms,” in *Asilomar Conference on Signals, Systems and Computers*, (2013).

18 J. Goodman, *Introduction to Fourier Optics*, MaGraw-Hill, 2 ed. (1996).

19 I. Yamaguchi, J. Kato, S. Ohta, and J. Mizuno, “Image formation in phase-shifting digital holography and applications to microscopy,” *Applied Optics* **40**, 6177–6186 (2001).

20 D. Salomon, *Data Compression: The Complete Reference*, Springer-Verlag New York, Inc., Secaucus, NJ, USA (2006).

21 G. A. Mills and I. Yamaguchi, “Effects of quantization in phase-shifting digital holography,” *Applied Optics* **44**, 1216–1225 (2005).

22 A. Arrifano, M. Antonini, and M. Pereira, “Multiple description coding of digital holograms using maximum-a-posteriori,” in *European Workshop on Visual Information Processing*, 232–237 (2013).

23 Y.-H. Seo, H.-J. Choi, and D.-W. Kim, “3D scanning-based compression technique for digital hologram video,” *Image Communication* **22**, 144–156 (2007).

24 E. Darakis and T. J. Naughton, “Compression of digital hologram sequences using MPEG-4,” in *Proc. SPIE, Holography: Advances and Modern Trends*, **7358**, 735811 (2009).

25 A. Benazza-Benyahia, J.-C. Pesquet, and M. Hamdi, “Vector lifting schemes for lossless coding and progressive archival of multispectral images,” *IEEE Transactions on Geoscience and Remote Sensing* **40**, 2011–2024 (2002).

26 M. Kaaniche, A. Benazza-Benyahia, B. Pesquet-Popescu, and J.-C. Pesquet, “Vector lifting schemes for stereo image coding,” *IEEE Trans. on Image Proc.* **18**(11), 2463–2475 (2009).

27 M. Moellenhoff and M. Maier, "Transform coding of stereo image residuals," *IEEE Transactions on Image Processing* **7**, 804–812 (1998).

28 N. V. Boulgouris and M. G. Strintzis, "A family of wavelet-based stereo image coders," *IEEE Transactions on Circuits and Systems for Video Technology* **12**(10), 898–903 (2002).

29 W. Sweldens, "The lifting scheme: A custom-design construction of biorthogonal wavelets," *Applied and computational harmonic analysis* **3**(2), 186–200 (1996).

30 F. J. Hampson and J.-C. Pesquet, "M-band nonlinear subband decompositions with perfect reconstruction," *IEEE Transactions on Image Processing* **7**(11), 1547–1560 (1998).

31 M. Kaaniche, A. Benazza-Benyahia, B. Pesquet-Popescu, and J.-C. Pesquet, "Non separable lifting scheme with adaptive update step for still and stereo image coding," *Elsevier Signal Processing: Special issue on Advances in Multirate Filter Bank Structures and Multiscale Representations* **91**, 2767–2782 (2011).

32 M. Kaaniche, B. Pesquet-Popescu, A. Benazza-Benyahia, and J.-C. Pesquet, "Adaptive lifting scheme with sparse criteria for image coding," *Journal on Advances in Signal Processing: Special issue on New Image and Video Representations Based on Sparsity* **2012** (2012).

33 R. R. Coifman and M. V. Wickerhauser, "Entropy-based algorithms for best basis selection.," *IEEE Transactions on Information Theory* **38**(2), 713–718 (1992).

34 D. Taubman and M. Marcellin, *JPEG2000: Image Compression Fundamentals, Standards and Practice*, Kluwer Academic Publishers, Norwell, MA, USA (2001).

35 Z. Wang, A. C. Bovik, H. R. Sheikh, and E. P. Simoncelli, "Image quality assessment: From error visibility to structural similarity," *IEEE Trans. on Image Processing* **13**, 600–612 (2004).

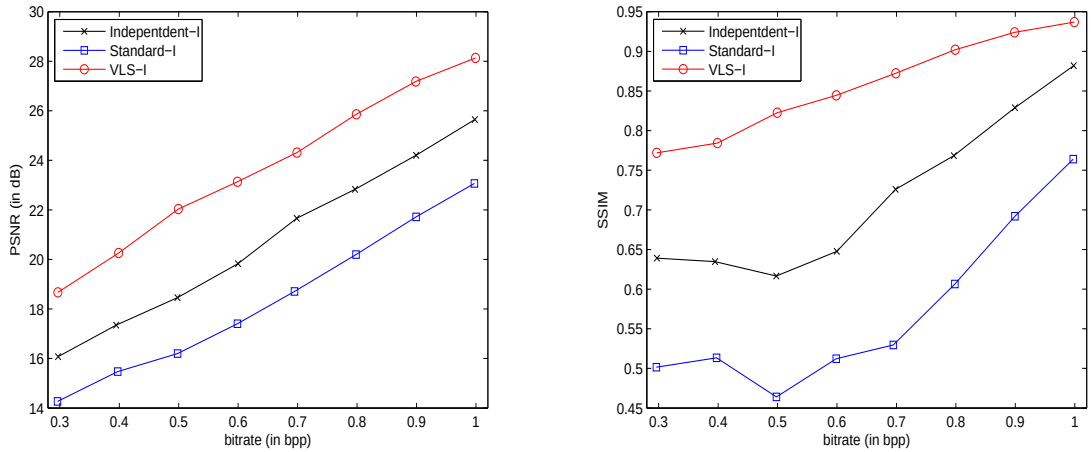


(a)

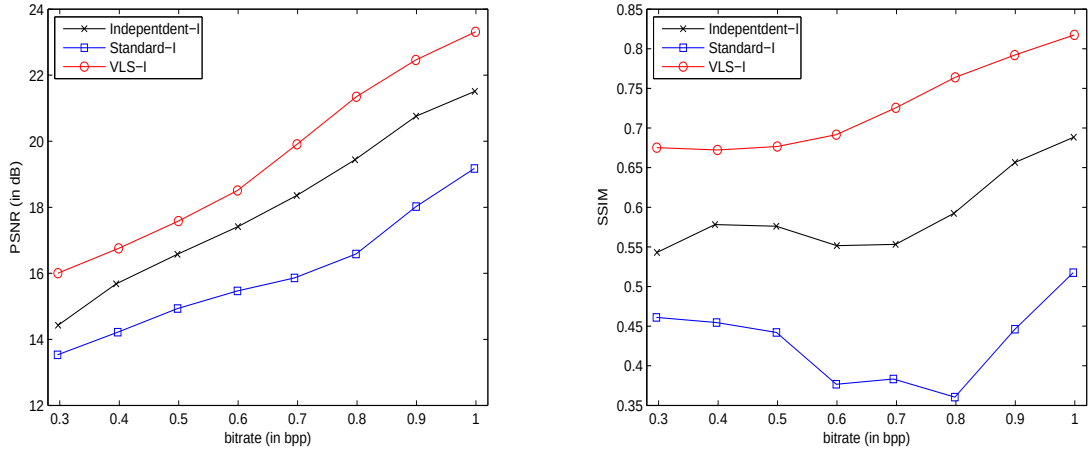


(b)

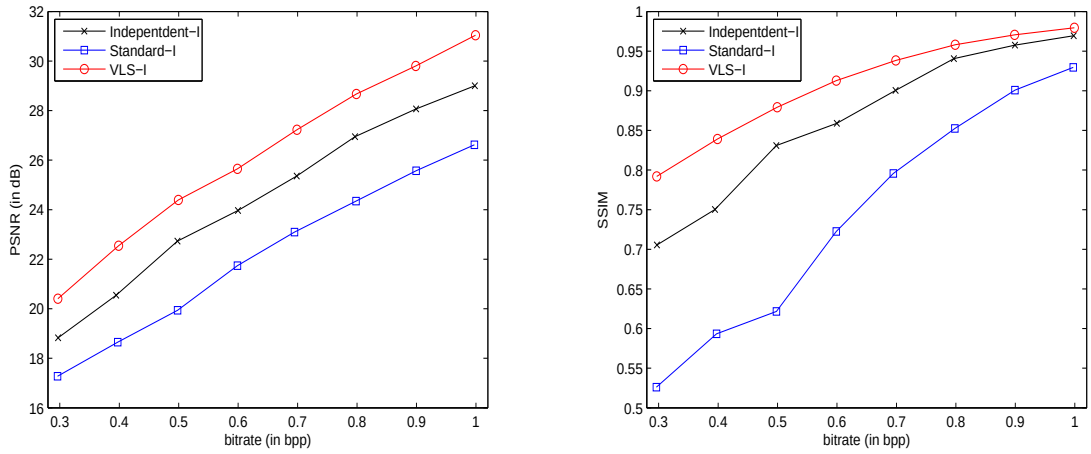


(c)

**Fig 6** Rate-distortion performance of the different hologram compression schemes applied on $D^{(1)}$ and $D^{(2)}$ for the objects: (a) “Bunny-1”, (b) “Bunny-2”, (c) “Girl”.

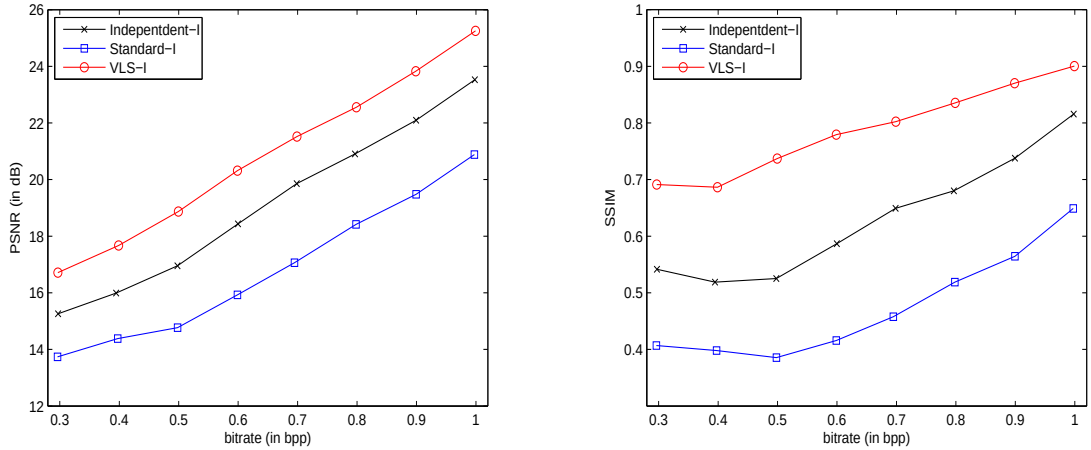


(a)

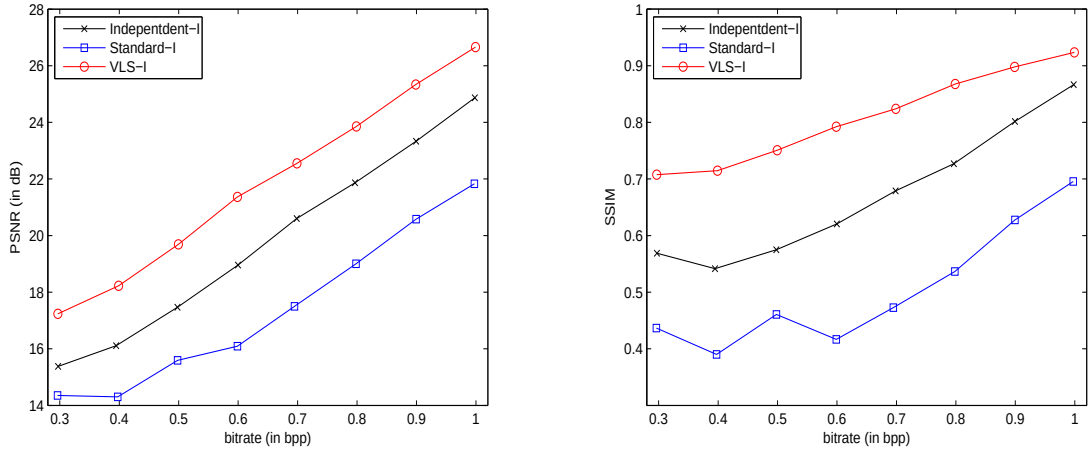


(b)

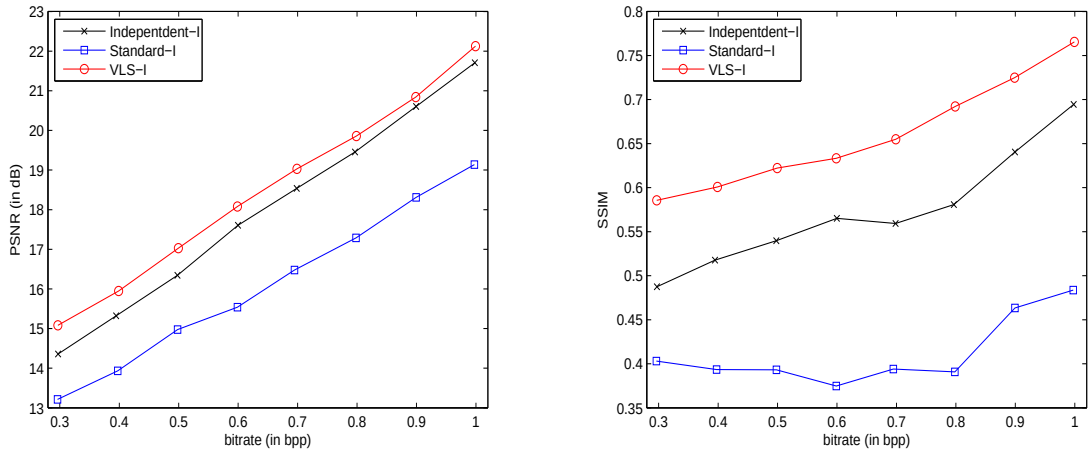


(c)

**Fig 7** Rate-distortion performance of the different hologram compression schemes applied on $D^{(1)}$ and $D^{(2)}$ for the objects: (a) “Luigi-1”, (b) “Luigi-2”, (c) “Teapot”.

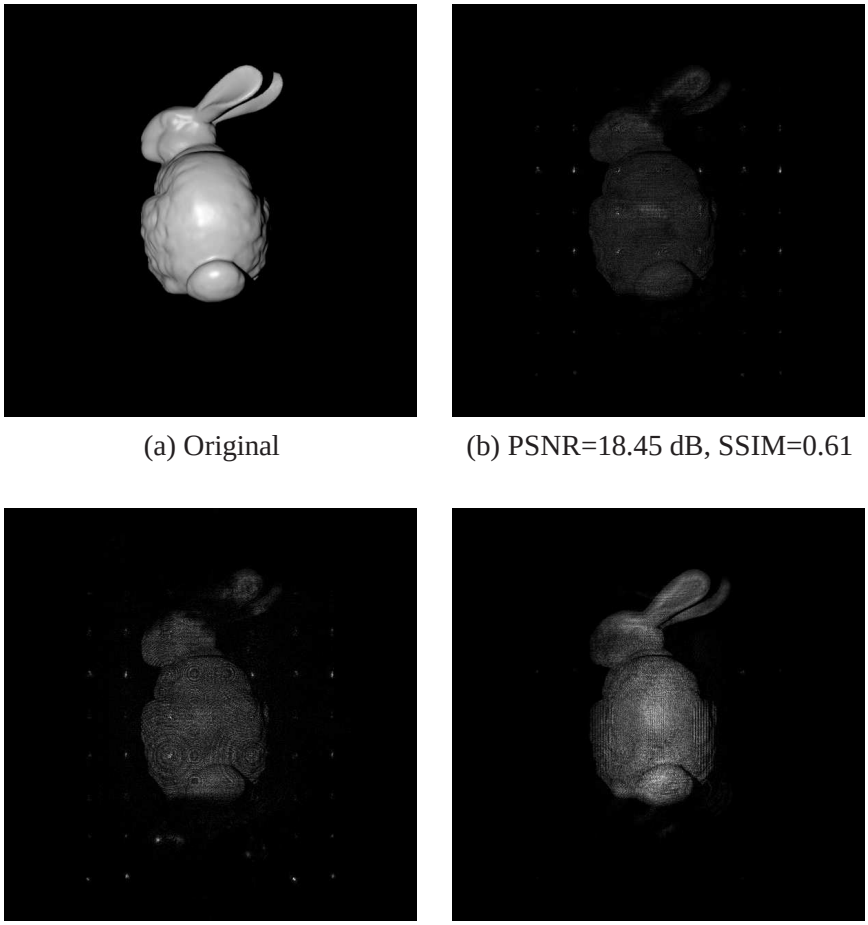

(a) Original (b) PSNR=18.45 dB, SSIM=0.61

(c) PSNR=16.19 dB, SSIM=0.46 (d) PSNR=22.03 dB, SSIM=0.82

**Fig 8** Reconstructed “Bunny-1” object at 0.5 bpp using: (a): Original, (b) Independent-I, (c) Standard-I, (d) VLS-I.

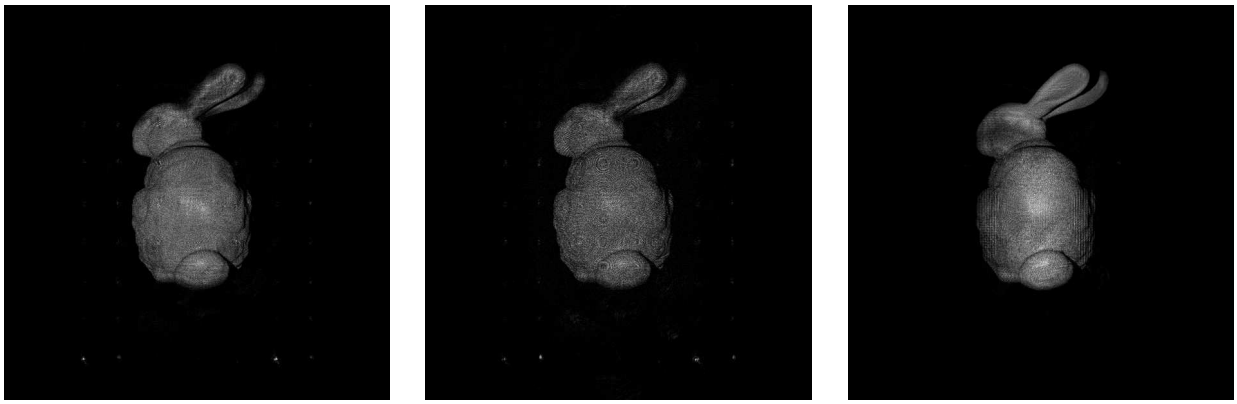

(a) PSNR=21.65 dB, SSIM=0.72 (b) PSNR=18.70 dB, SSIM=0.52 (c) PSNR=24.32 dB, SSIM=0.87

**Fig 9** Reconstructed “Bunny-1” object at 0.7 bpp using: (a) Independent-I, (b) Standard-I, (c) VLS-I.

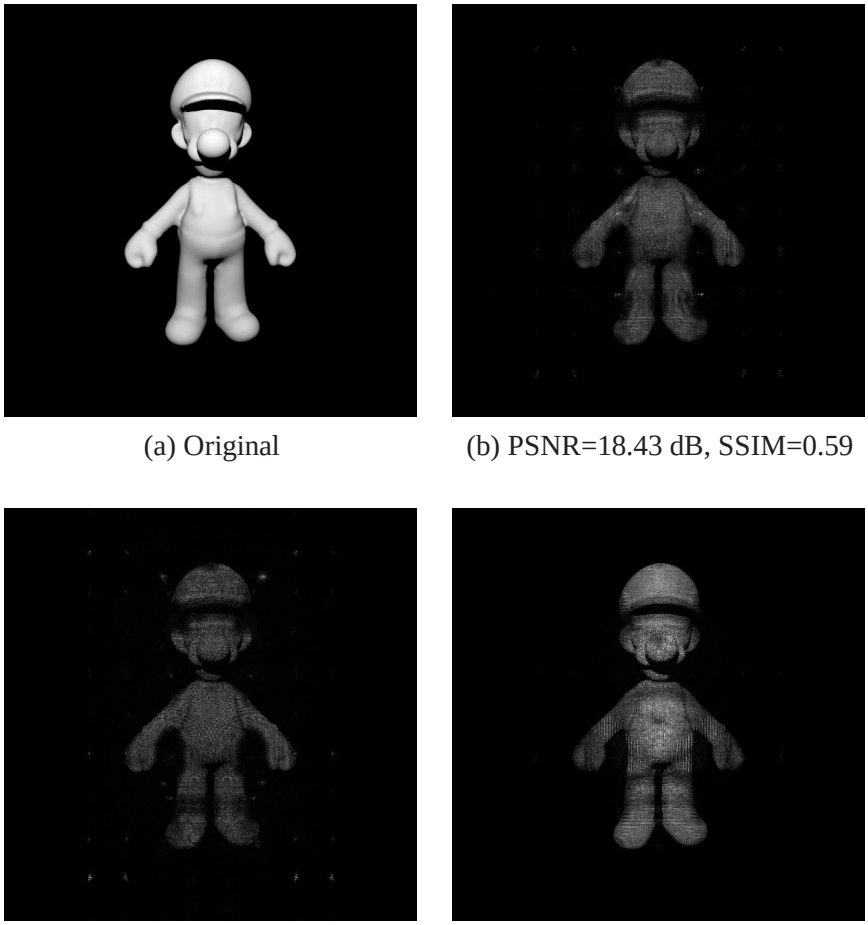

(a) Original (b) PSNR=18.43 dB, SSIM=0.59

(c) PSNR=15.93 dB, SSIM=0.42 (d) PSNR=20.31 dB, SSIM=0.78

**Fig 10** Reconstructed “Luigi-1” object at 0.6 bpp using: (a) Original, (b) Independent-I, (c) Standard-I, (d) VLS-I.

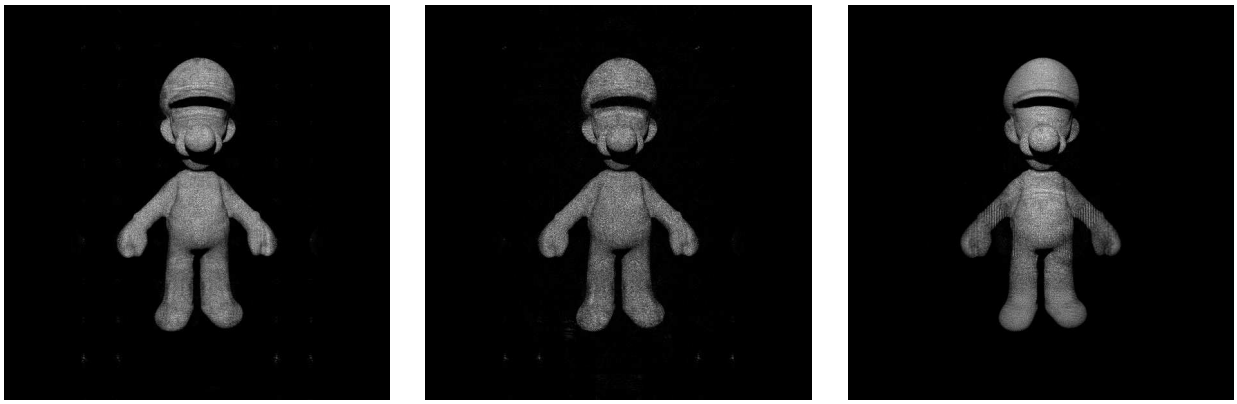

(a) PSNR=22.10 dB, SSIM=0.74 (b) PSNR=19.48 dB, SSIM=0.56 (c) PSNR=23.83 dB, SSIM=0.87

**Fig 11** Reconstructed “Luigi-1” object at 0.9 bpp using: (a) Independent-I, (b) Standard-I, (c) VLS-I.

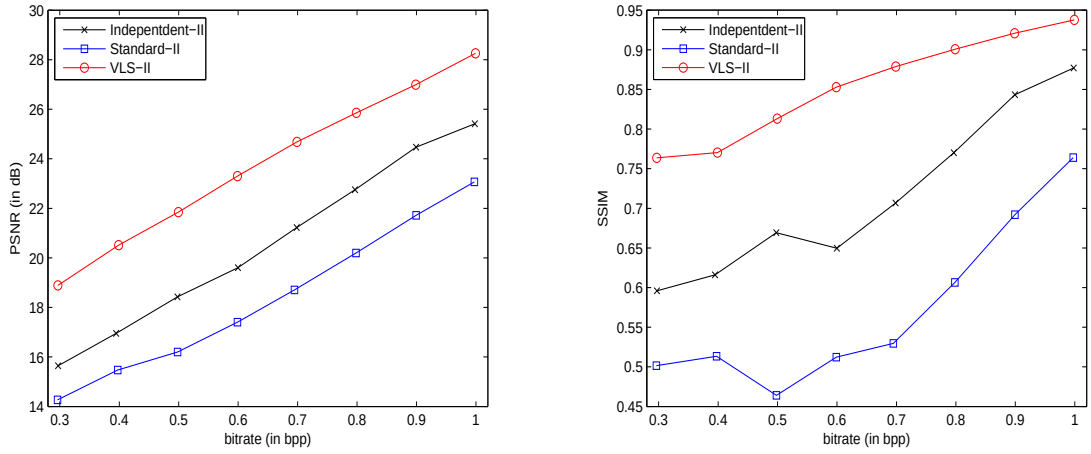


(a)

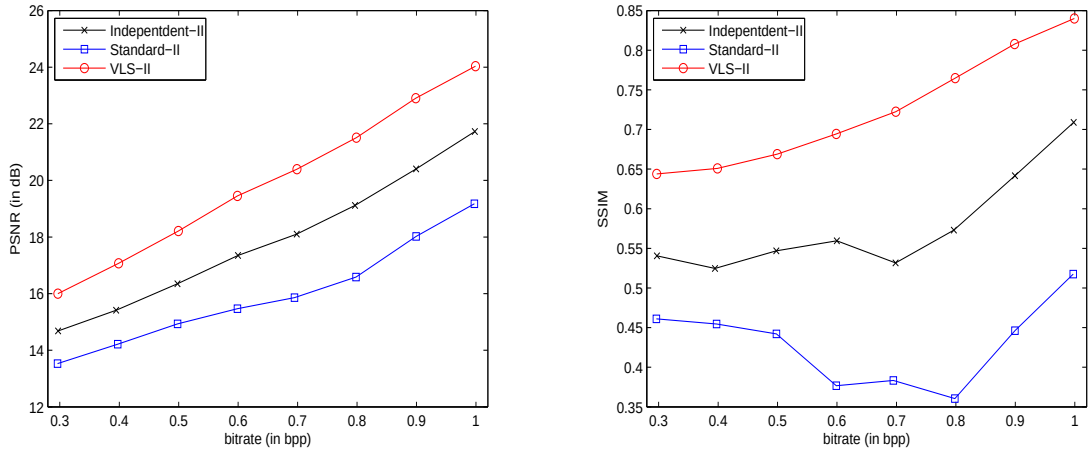


(b)

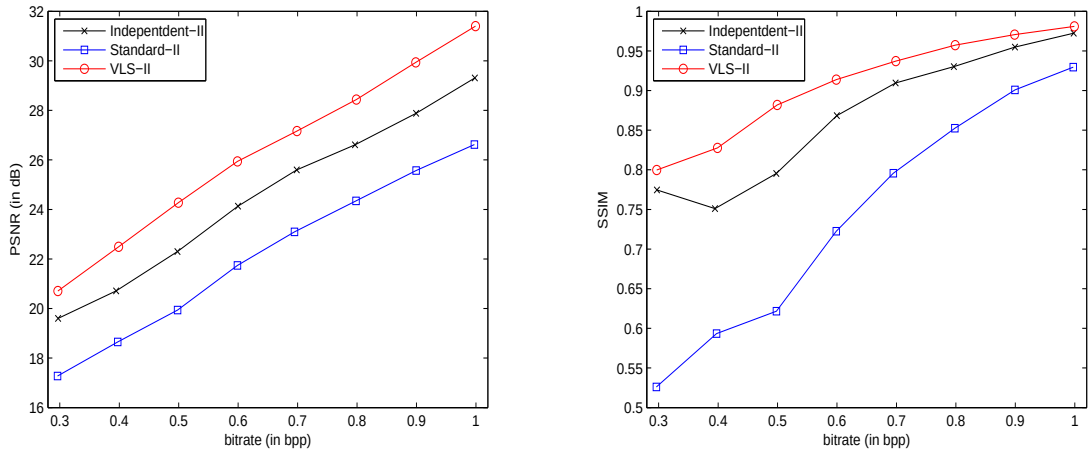


(c)

**Fig 12** Rate-distortion performance of the different hologram compression schemes applied on $I^{(1)}$ and $I^{(2)}$ for the objects: (a) “Bunny-1”, (b) “Bunny-2”, (c) “Girl”.

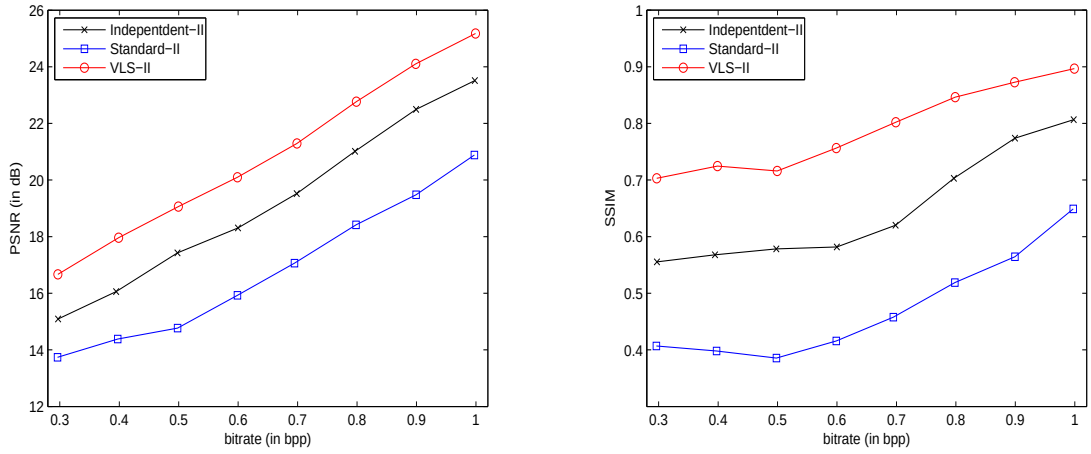


(a)

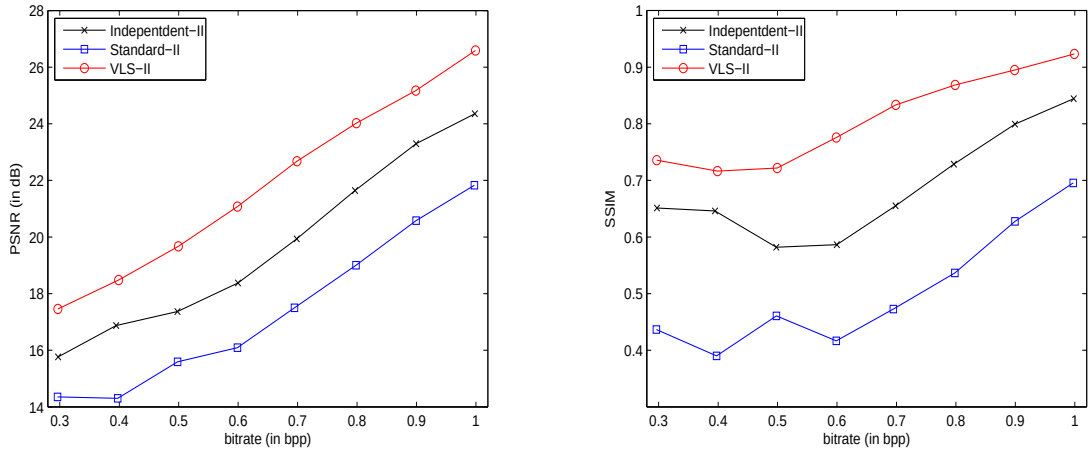


(b)

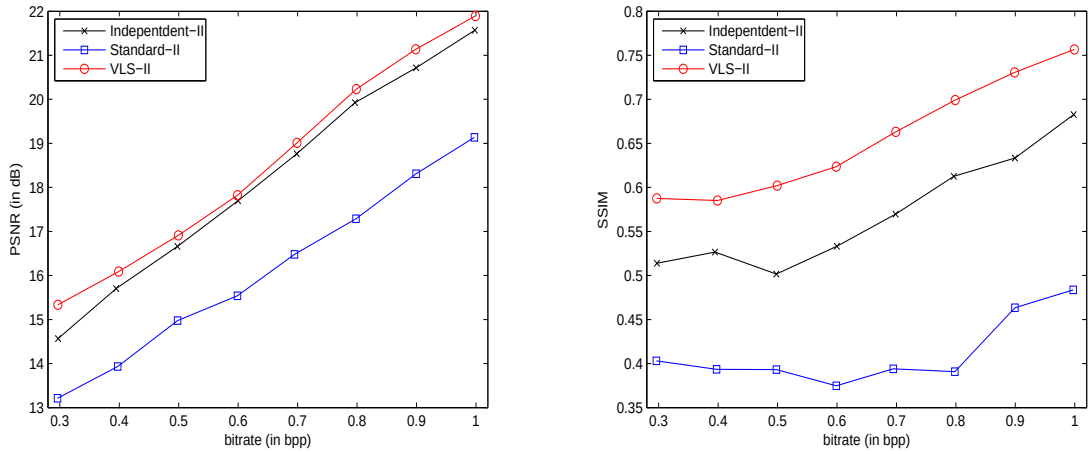


(c)

**Fig 13** Rate-distortion performance of the different hologram compression schemes applied on $I^{(1)}$ and $I^{(2)}$ for the objects: (a) “Luigi-1”, (b) “Luigi-2”, (c) “Teapot”.